Emergent flat band lattices in spatially periodic magnetic fields

M. Tahir,[1] Olivier Pinaud,[2] and Hua Chen[1,3]
[1]*Department of Physics, Colorado State University, Fort Collins, Colorado 80523, USA*
[2]*Department of Mathematics, Colorado State University, Fort Collins, Colorado 80523, USA*
[3]*School of Advanced Materials Discovery, Colorado State University, Fort Collins, Colorado 80523, USA*

(Received 4 September 2018; revised 20 June 2020; accepted 25 June 2020; published 20 July 2020)

Motivated by the recent discovery of the Mott insulating phase and unconventional superconductivity due to the flat bands in twisted bilayer graphene, we propose more generic ways of getting two-dimensional (2D) emergent flat-band lattices using either 2D Dirac materials or ordinary electron gas (2DEG) subject to moderate periodic orbital magnetic fields with zero spatial average. We find stark contrast between Schrödinger and Dirac electrons, i.e., the former show recurring "magic" values of the magnetic field when the lowest band becomes flat, whereas, for the latter, the zero-energy bands are asymptotically flat without magicness. By examining the Wannier functions localized by the smooth periodic magnetic fields, we are able to explain these nontrivial behaviors using minimal tight-binding models on a square lattice. In particular the magicness of the 2DEG can be understood in terms of destructive quantum interference similar to classic flat-band lattice models. The two cases can be interpolated by varying the g factor or effective mass of a 2DEG and by taking into account the Zeeman coupling, which also leads to flat bands with nonzero Chern numbers for each spin. Our paper provides flexible platforms for exploring interaction-driven phases in 2D systems with on-demand superlattice symmetries.

DOI: 10.1103/PhysRevB.102.035425

I. INTRODUCTION

Moiré structures formed by stacking two-dimensional (2D) crystals, such as graphene, hexagonal boron nitride, transition-metal dichalcogenides, etc., have attracted a lot of attention recently [1–5]. For incommensurate moiré structures, in-plane translation symmetry is broken, posing challenges to the paradigm of solid-state physics based on Bloch's theorem. Nonetheless, in the long-wavelength limit and when the moiré potential is weak, one can still adopt a momentum-space description of the low-energy electronic states, and obtain "moiré band structures" even in the case of incommensuration [6–8]. In this context, Bistritzer and MacDonald first found that the moiré structure formed by twisted bilayer graphene has flat bands at charge neutrality for certain "magic angles" of twisting [8]. The strongly suppressed kinetic energy in these flat bands suggests potential for interaction-driven exotic phases, which were recently revealed experimentally in Refs. [9–11] where both correlated insulating and unconventional superconducting ($T_c \sim 1$ K) phases were found near charge neutrality in twisted bilayer graphene at the first magic angle $\theta \approx 1.05^\circ$.

Although the flat moiré bands in the family of twisted multilayer van der Waals materials [12–14] may host other interaction-driven phases, these phases will inevitably be restricted or selected by the symmetries of the moiré structures, which determine the form of interactions in the moiré bands [15–28]. The spatial symmetry of a moiré structure, however, cannot be easily changed since it is dictated by the crystal symmetry of the constituent layers. For example, the moiré pattern of twisted bilayer graphene always has the form of a triangular lattice with a sixfold rotation symmetry. One main task of this paper is to provide practical ways of realizing 2D flat bands with different crystalline symmetries by design, *not* relying on moiré structures, thus, enabling exploration of exotic phases in a larger parameter space. This is made possible through a more generic understanding of the origin of moiré flat bands, which motivates us to replace the moiré potential [29–31] by periodic external magnetic fields or other artificial crystal potentials, such as Zeeman or strain fields [32–35], that can now be created and controlled experimentally.

There has been a long effort of creating spatially periodic electric and magnetic fields and studying their influence on condensed-matter systems. One of the earliest examples is the observation of Weiss oscillations in conventional two-dimensional electron gas (2DEG) in GaAs/AlGaAs subject to a one-dimensional (1D) periodic static electric potential, created by parallel fringes or metallic strip arrays, and a perpendicular homogeneous magnetic field [36], which is due to the commensuration between the cyclotron radius and the period of the electric potential [37–40]. Two-dimensional periodic electric potentials on 2DEG [41–45] with different symmetries [46–48] were also realized, which show Hofstadter butterfly spectra under moderate homogeneous magnetic fields. In parallel, spatially periodic (orbital) magnetic fields in 1D [49–52], 2D [53–56], and Zeeman fields [57] have been experimentally realized using periodic arrays of superconducting or ferromagnetic strips or dots. More recently, 1D [58] and 2D [59–61] periodic electric potentials have also been realized in graphene.

In this paper, we propose that 2D-periodic magnetic fields with zero average, applied on either 2D Dirac systems or ordinary 2DEG, are an effective and versatile way of creating flat bands with different superlattice symmetries in the low-energy electronic structure. Studies on 1D-periodic magnetic fields

with zero average exist in literature [33,62–67], but no general conclusions have been made on the existence and origin of 2D flat bands in nonquantizing 2D periodic magnetic fields. We find that, for a simple 2D sinusoidal magnetic field forming a square Bravais lattice, Schrödinger and Dirac electrons exhibit drastically different behaviors in the tendency of realizing flat low-energy bands: The lowest band for the Schrödinger electron (or 2DEG) becomes flat repeatedly at magic values of the dimensionless parameter $\phi \equiv eB/\hbar K^2$, where B is the amplitude of the periodic magic field and K is the reciprocal lattice constant. In contrast, the two particle-hole-symmetric bands near zero energy of the Dirac electron only become asymptotically flat with increasing ϕ without magicness. The different behaviors of the two systems can be understood by looking into the Wannier functions of the low-energy bands and the accompanying tight-binding Hamiltonians. Although, in the Dirac case, the lowest bands can be described by Gaussian-like Wannier functions localized around the centers of square plaquettes with a definite sign of the magnetic field, in the Schrödinger case, the lowest bands are best described by two Gaussian-like Wannier functions localized at the corners of a square plaquette. As a result, the nearest-neighbor hopping for the Schrödinger case is complex and varies with ϕ in an oscillatory way, and, at special values of ϕ, the kinetic energy vanishes due to destructive interference, which explains the magicness. Such a mechanism is reminiscent of the classic examples of flat-band lattice models [68–73] and can be captured by a minimal tight-binding model. On the other hand, in the Dirac case, the nearest-neighbor hopping between Wannier functions at plaquettes centers is real and becomes monotonically smaller as ϕ increases. Moreover, by taking into account Zeeman coupling and spin degrees of freedom, one can naturally interpolate between Dirac and Schrödinger electrons, by varying the g factor or the effective mass of a 2DEG. In this case, we find that it is common for the lowest flat band to have a nonzero Chern number for each spin species, despite the magnetic field having zero spatial average. Such a behavior can be qualitatively described by a three-band model. Our paper, thus, provides flexible platforms for realizing 2D flat-band systems with different superlattice symmetries and nontrivial topology for exploring exotic interaction-driven phases.

The remainder of this paper is organized as follows: In Sec. II, we solve the periodic magnetic-field problem for Dirac and Schrödinger electrons using momentum-space and real-space numerical methods and reveal the flat-band behaviors. For the Dirac case, we also provide an analytic solution which checks with the numerical results. In Sec. III, we obtain the maximally localized Wannier functions for the flat bands in both cases, based on which we construct Gaussian-like Wannier functions that can give physically intuitive real-space tight-binding Hamiltonians. In Sec. IV, we provide minimal nearest-neighbor tight-binding models based on the information of the Wannier functions obtained in Sec. III, which can explain the contrasting behaviors of the two systems. In Sec. V, we study the effect of Zeeman coupling of the periodic magnetic field and show that the isolated low-energy flat band can quite often have a nonzero (spin) Chern number. Based on the knowledge of the Wannier functions of the low-energy bands, we construct a minimal three-band model that can describe this behavior. Brief discussions and conclusions are given in Sec. VI.

II. BAND FLATTENING FOR DIRAC AND SCHRöDINGER ELECTRONS IN PERIODIC MAGNETIC FIELDS

A. Dirac electron

We start by considering a generic 2D Dirac system subject to a perpendicular magnetic field having two cosinusoidal components along the x and y directions, respectively: $\mathbf{B} = B[\cos(Kx) + \cos(Ky)]\hat{z}$, where $K \equiv 2\pi/a$ is the wave number with a as the period of the magnetic modulation. Specific material realizations and effects of more complex functional forms of fields will be discussed later. The single-particle Hamiltonian is

$$H^D = v_F \boldsymbol{\sigma} \cdot \boldsymbol{\Pi}, \tag{1}$$

where v_F is the Fermi velocity of the Dirac electron, $\boldsymbol{\Pi} = -i\hbar\boldsymbol{\nabla} + e\mathbf{A}$ is the kinetic momentum with e as the absolute value of electron charge, and $\boldsymbol{\sigma} = \sigma_x\hat{x} + \sigma_y\hat{y}$. The vector potential $\mathbf{A}$ corresponding to the periodic magnetic field in the Coulomb gauge is

$$\mathbf{A} = \frac{B}{K}[-\sin(Ky)\hat{x} + \sin(Kx)\hat{y}]. \tag{2}$$

For such a simple vector potential, it is convenient to use plane-wave expansion to solve the eigenvalue problem [8] (see the Supplemental Material [74]). The momentum-space Hamiltonian is an infinite-dimensional sparse matrix with a single-dimensionless parameter $\phi \equiv eB/\hbar K^2$ determining the strength of the magnetic potential. To obtain the band structure, one has to truncate the momentum-space Hamiltonian by choosing an appropriate bound of reciprocal lattice vectors $\mathbf{K}$ for a given ϕ so that the low-energy band structure is converged. We have used a cutoff of the form $\max(|K_x|, |K_y|) \leqslant K_c$ and found that convergence for moderate values of $\phi \sim 1$ can be well achieved with $K_c = 5$. As has been noted previously [8,75], such a plane-wave expansion method does not require ϕ to be small as long as K_c is large enough.

The Dirac Hamiltonian Eq. (1) with the periodic vector potential Eq. (2) has a particle-hole symmetry: $\sigma_z H^D \sigma_z = -H^D$ and a zero-energy solution. By diagonalizing the truncated Hamiltonian and focusing on the two particle-hole symmetric bands near zero energy, we found that the velocity near zero momentum monotonically decreases with increasing ϕ and approaches zero asymptotically as shown in Fig. 1. The two low-energy bands are separated from other bands, and their overall bandwidth is monotonically decreasing. Thus, one can get as flat as possible low-energy bands by keeping increasing ϕ without fine-tuning. Moreover, the flatness is controlled by $\phi = eB/\hbar K^2$ instead of B alone and can, thus, be large by having a large period even with a relatively small B. Quantitative estimates, including lower bounds on the magnetic field set by the disorder potential, will be given in the Discussion.

Such behavior of Dirac electrons in periodic magnetic fields can also be obtained analytically by perturbing the zero-energy eigensolution of H^D with $\hbar v_F \boldsymbol{\sigma} \cdot \mathbf{k}$, where $\mathbf{k}$ is a small wave vector [76,77] and the Supplemental Material [74]. This gives a renormalized Fermi velocity $v_F^{\text{eff}} = v_F/[I_0(2\phi)]^2$, where I_0 is the zeroth modified Bessel function of the first

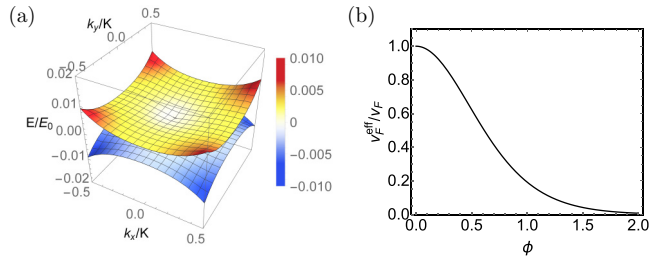

FIG. 1. Flat bands for Dirac electrons in periodic magnetic fields. (a) Band structure for the two particle-hole symmetric bands close to zero energy when $\phi = 2$. $E_0 = \hbar v_F K$ is the energy unit. The color scale is the same as E/E_0. (b) Renormalized Fermi velocity $v_F^{\rm eff}$ vs ϕ. A plane-wave cutoff of $K_c = 5\ K$ is used.

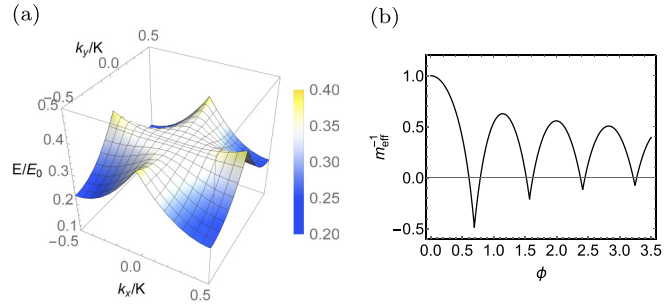

FIG. 2. Flat bands for 2DEG in periodic magnetic fields. (a) Band structure for the lowest band when $\phi = 0.6$ near the first magic value. $E_0 = \hbar^2 K^2/2m$ is the energy unit. The color scale is the same as E/E_0 with white corresponding to the energy at $\mathbf{k} = 0$. (b) Renormalized inverse effective-mass $m_{\rm eff}^{-1}$ (in units of m^{-1}) vs ϕ. A plane-wave cutoff of $K_c = 9\ K$ is used.

kind. At large ϕ, $v_F^{\rm eff}$ takes the asymptotic form $4\pi\phi e^{-4\phi} v_F$. For a triangular lattice periodic magnetic field, we did not find an analytic expression of $v_F^{\rm eff}$, but numerical calculation shows that the band-flattening behavior is qualitatively the same as the square lattice case (see the Supplemental Material [74]). Thus, periodic magnetic fields can be used as an effective way of creating flat band Dirac systems with different superlattice symmetries.

On the other hand, when $\phi \ll 1$, one can also obtain an effective 2×2 Hamiltonian using perturbation theory and keeping the lowest order in ϕ. Such a calculation (see the Supplemental Material [74]) shows that $v_F^{\rm eff} \approx (1 - \phi^2) v_F$ which describes the quadratic behavior of $v_F^{\rm eff}(\phi)$ at small ϕ in Fig. 1. When $\phi \gtrsim 1$, the perturbation theory obviously breaks down, but $\phi \sim 1$ can, nevertheless, be viewed as a critical scale of the magnetic field at which $v_F^{\rm eff}(\phi)$ starts to decay exponentially.

We note that $v_F^{\rm eff} = 0$ does not necessarily mean the corresponding bands are flat throughout the Brillouin zone. In practice, flat bands are interesting mainly because they lead to diverging density of states (DOS) which makes correlation effects most pronounced. $v_F^{\rm eff} = 0$ at $\mathbf{k} = 0$ is not a sufficient condition for diverging density of states. However, for the smooth potential profile considered here, the overall flattening of the lowest band throughout the Brillouin zone is consistent with the behavior near $\mathbf{k} = 0$. This can be seen, for example, by looking at the momentum-space Hamiltonian at the Brillouin-zone boundary. The lowest bands at $\mathbf{k} = \frac{1}{2}\hat{x}$ are doubly degenerate in the absence of the magnetic field and have energies $\epsilon = \pm 1/2$. In each of the twofold degenerate subspaces, the magnetic field induces a splitting proportional to $\phi/2$. We note, in passing, that a periodic scalar potential does not split the two doublets, which is another reason why periodic magnetic fields are special in getting flat bands. Thus, $\phi \sim 1$ is a crude estimate of when the lowest bands become very close to zero energy at the Brillouin-zone boundary. (The estimate based on degenerate perturbation breaks down when $\phi \gtrsim 1$.) For a smooth vector potential, such as Eq. (2), the lowest bands are not expected to vary strongly throughout the Brillouin zone. Thus, the monotonic decrease of $v_F^{\rm eff}$ at $\mathbf{k} = 0$ together with the approaching of low-energy bands towards 0 at zone boundary suggest the overall flattening of the lowest band and the diverging density of states as ϕ increases. To provide additional support of the claims above, we have plotted the bandwidth of the lowest positive energy band in Fig. 1 of the Supplemental Material [74]. The trend of bandwidth narrowing in the Dirac case is faithfully reflected by the reduction of velocity at $\mathbf{k} = 0$.

Another consequence of the flat band, at least, near $\mathbf{k} = 0$, is the immobility of the wave packet centered around $\mathbf{k} = 0$. Physically, it means that particles described by such wave packets will be easily trapped or localized by disorder. This is formally considered as the homogenization problem in partial differential equation theory, which absorbs the effect of a periodic potential into an effective-mass tensor by considering the dynamics at a much larger scale than the period. There is a great amount of literature on the subject in the Schrödinger case, see, e.g., Refs. [78,79] for some rigorous mathematical references. The situation is similar for the Dirac equation under appropriate assumptions, which will be addressed in a future work [80]. In this context, the vanishing $v_F^{\rm eff}$ directly corresponds to flat bands for the Dirac operator.

B. Schrödinger electron

We next show that periodic magnetic fields can lead to flat bands for 2D Schrödinger electrons but only at discrete values of the parameter ϕ. Using the same vector potential Eq. (2), the Hamiltonian is

$$H^S = \frac{1}{2m}\mathbf{\Pi}^2, \tag{3}$$

where m is the effective mass of electrons in a given system. By diagonalizing the momentum-space Hamiltonian with a large enough cutoff, we calculate the inverse effective mass of the lowest band $m_{\rm eff}^{-1}$ at $\mathbf{k} = 0$ and plot it against ϕ. Figure 2(b) shows that $m_{\rm eff}^{-1}$ has an oscillatory dependence on ϕ and crosses zero repeatedly as ϕ increases. In Figs. 1 and 2 of the Supplemental Material [74], we show that, although the bandwidth of the lowest band is nonzero when $m_{\rm eff}^{-1}(\mathbf{k} = 0)$ vanishes, it reaches local minima at these points, accompanied by diverging density of states at the energy of the lowest band at $\mathbf{k} = 0$. In the more generalized context mentioned above, it is still reasonable to be called flat bands at these magic values.

Our real-space calculation using the spectral method gives the same result (see the Supplemental Material [74]). Our

calculations for a triangular lattice periodic magnetic field also show similar oscillatory behavior [74]. Later in the Discussion, we will show that the qualitative behavior is retained even for more realistic Gaussian-like magnetic-field profile. Thus, in contrast to Dirac electrons, 2DEG can have flat bands with exact vanishing of m_{eff}^{-1} at magic values of ϕ.

For Schrödinger electrons, we are not able to find an analytic solution of the lowest band. However, since the smallest magic value of $\phi \approx 0.6$ is less than 1, second-order perturbation may still be valid near this value (see the Supplemental Material [74]). The effective Hamiltonian, thus, obtained is

$$H_{\text{eff}}^{S}(\mathbf{k}) = k^2(1 - 2\phi^2) + \phi^2. \tag{4}$$

The inverse mass vanishes when $\phi = \frac{1}{\sqrt{2}} \approx 0.707$, which is off by only about 15%. That the second-order perturbation is approximately valid can also be seen from the exact result in Fig. 2(b), which shows that, before reaching its first minimum, m_{eff}^{-1} is roughly quadratic in ϕ. Since the quadratic ϕ dependence in Eq. (4) is accurate when $\phi \to 0$, it should serve as a good approximation until the behavior of $m_{\text{eff}}^{-1}(\phi)$ significantly changes. However, to understand the origin of the recurring magic values in the Schrödinger case and why there is no magicness in the Dirac case, we have to look into details of the wave functions associated with the flat bands.

III. WANNIER FUNCTIONS OF THE FLAT BANDS

We next examine the Wannier functions associated with the lowest bands for both Schrödinger and Dirac electrons and, based on them, explain the contrasting band-flattening behaviors using minimal tight-binding models. We note that Wannier functions localized by periodic magnetic fields is by itself an interesting problem as historically the discussion on the effect of magnetic fields on Wannier functions is mostly focused on slow-varying magnetic fields on the length scale of the Wannier functions or, equivalently, of the lattice constants [81–83] in crystalline solids. In this case, the effect of magnetic fields can be approximately described as the Peierls phase in the Hamiltonian written in the basis of Wannier functions, and the Wannier functions themselves are only slightly modified through a phase factor. In the present systems, however, the "lattice constant" is set by the spatial period of the magnetic field, and the slow-variation assumption cannot be justified *a priori*.

We first consider the Schrödinger case. We found that the absolute value of the maximally localized Wannier function (MLWF) of the lowest band has four peaks at $\pm\frac{\pi}{K}\hat{x}$ and $\pm\frac{\pi}{K}\hat{y}$, which are minima of $|\mathbf{A}|^2$ (see the Supplemental Material [74]). This suggests that it may be possible to use a basis of two Gaussian-like Wannier functions, located at the plaquette corners $(\pi/K, 0)$ and $(0, \pi/K)$ to describe the lowest band. We, thus, project $\psi_{1\mathbf{k}}$ and $\psi_{2\mathbf{k}}$, Bloch functions of the two lowest bands, onto two Gaussians g_A and g_B located at $(\pi/K, 0)$ and $(0, \pi/K)$, respectively,

$$\begin{aligned}\phi_{A\mathbf{k}}(\mathbf{r}) &= \langle g_A|\psi_{1\mathbf{k}}\rangle\psi_{1\mathbf{k}}(\mathbf{r}) + \langle g_A|\psi_{2\mathbf{k}}\rangle\psi_{2\mathbf{k}}(\mathbf{r}),\\ \phi_{B\mathbf{k}}(\mathbf{r}) &= \langle g_B|\psi_{1\mathbf{k}}\rangle\psi_{1\mathbf{k}}(\mathbf{r}) + \langle g_B|\psi_{2\mathbf{k}}\rangle\psi_{2\mathbf{k}}(\mathbf{r}),\end{aligned} \tag{5}$$

which are then orthonormalized. Even though we did not run the maximal localization routine (see the Supplemental Material [74]), the tight-binding Hamiltonian in this basis has fast decaying hopping parameters with increasing distance (see the Supplemental Material [74]), and the interpolated band structure from this Hamiltonian fits that obtained using the plane-wave method very well [Fig. 3(e)].

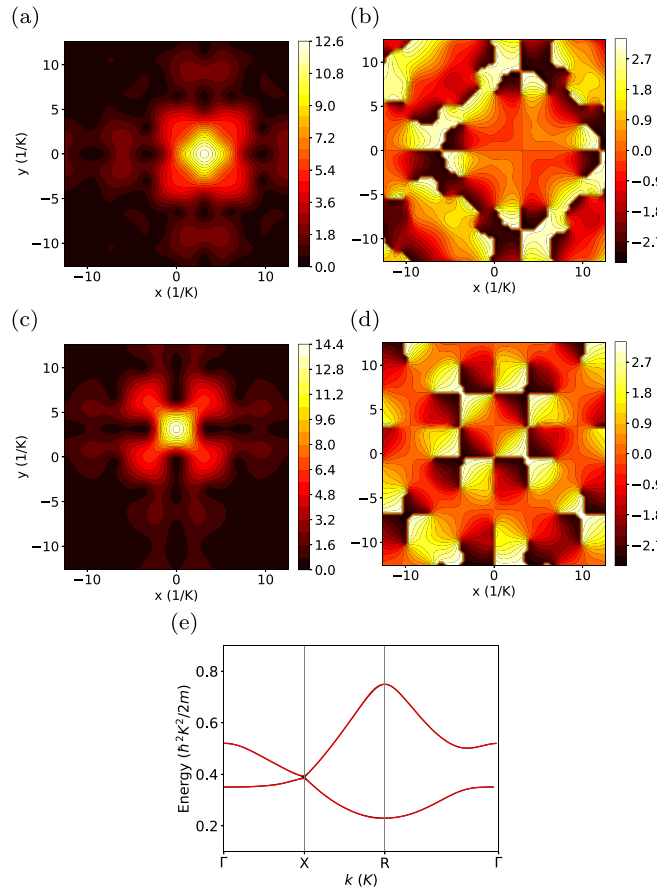

FIG. 3. Wannier functions of the two lowest bands of a Schrödinger electron. (a) and (b) Norm and phase of the first Wannier function ϕ_A located at $(\pi/K, 0)$. (c) and (d) Norm and phase of the second Wannier function ϕ_B located at $(0, \pi/K)$. (e) Wannier-interpolated band structure (red solid lines) compared with the plane-wave result (black solid lines). $\phi = 0.6$. A plane-wave cutoff of $K_c = 5\ K$ and a Brillouin-zone discretization of 11×11 were used. Widths of the two Gaussians used for constructing the Wannier functions are set at $8/K$.

Although the shapes of the two Wannier functions deviate from Gaussian-like after projection and orthonormalization, they are still localized at $(\pi/K, 0)$ and $(0, \pi/K)$. Moreover, each of them has a phase distribution qualitatively consistent with the Peierls form, i.e., the phase increases fastest along the lines with large line integral of the vector potential. One would then wonder if the real-space tight-binding Hamiltonian in the basis of these two Wannier functions also has complex hopping parameters with Peierls phases. We find that this is, indeed, the case. For example, the nearest-neighbor hopping from ϕ_A to ϕ_B at $\phi = 0.6$ is about $0.057i$ along $\pm(\hat{x} + \hat{y})$ and $-0.057i$ along $\pm(\hat{x} - \hat{y})$, which are mutually complex conjugate as expected from the behavior of $\exp(i\frac{e}{\hbar}\int \mathbf{A}\cdot d\mathbf{l})$. Moreover, it is surprising that the nearest-neighbor hopping is almost purely imaginary near the first magic value of ϕ.

These features provide important clues for our construction of a minimal tight-binding model below.

We next turn to the Wannier functions of the Dirac case. To describe Dirac and Schrödinger electrons in a unified manner, we make use of the particle-hole symmetry of the Dirac Hamiltonian H^D in Eq. (1) and consider its square $(H^D)^2$ (see the Supplemental Material [74]). In stark contrast to the Schrödinger case, the peaks of the MLWF of the lowest band are now located at $(\pm\pi/K, \pm\pi/K)$ (four equivalent points) and (0,0), which are the minima of $\pm B(\mathbf{r})$ for spin up and spin down, respectively [74]. Since the tight-binding Hamiltonians are one dimensional now, all the hopping parameters are real and monotonically decrease as ϕ increases. This is because the potential wells of $\pm B(\mathbf{r})$ become monotonically deeper, which also explains the asymptotic band-flattening behavior.

We note that, for both cases, the lowest band is touching the next lowest one at the Brillouin-zone boundary. For the Schrödinger case, the band touching is at the X point or $(k_x, k_y) = (1/2, 0)$ and its symmetry related points, whereas, for the Dirac case [either H^D or $(H^D)^2$], it is at the R point or (1/2,1/2) and its symmetry-related points. If such degeneracies are removed and the lowest band has a nonzero Chern number, which is possible because of the broken time-reversal symmetry in the present systems, exponentially localized Wannier functions for the lowest band cannot exist. We will discuss the Chern number in more detail below.

IV. MINIMAL TIGHT-BINDING MODELS FOR THE FLAT-BAND LATTICES

The Wannier functions obtained above motivate us to construct a minimal tight-binding model to explain the recurring magic values for the Schrödinger case. The model has spinless free fermions hopping between nearest neighbors on a 2D square lattice where the lattice sites coincide with the plaquette corners, i.e., positions of the Wannier functions in Fig. 3,

$$H = -\sum_{\langle ij\rangle} t e^{i\varphi_{ij}} c_i^\dagger c_j + 4t, \tag{6}$$

where $t = \hbar^2/2ma^2$ is the hopping parameter between nearest neighbors and the summation is over nearest neighbors. For convenience, we have rotated the coordinate system by $\pi/4$ around the z axis, compared to that used for Eq. (2). For the 2D-cosinusoidal magnetic field used above, the absolute value of the flux through a plaquette is $\Phi = 16B/K^2 = 8Ba^2/\pi^2$. All positive flux plaquettes only share edges with negative flux ones. The square lattice looks like a checkerboard with two sites per unit cell, and the black and white squares correspond to positive and negative magnetic fluxes of the same size [Fig. 4(a)]. Based on the spatial distribution of the phase of the Wannier functions, we expect it to be qualitatively correct to include the magnetic field as a Peierls phase in the hopping parameter, which is $e^{i\varphi_{ij}}$ in Eq. (7). Integrating the vector potential in Eq. (2) along the bonds gives the phase φ_{ij},

$$\varphi_{ij} = \pm\frac{4eB}{\hbar K^2} = \pm\frac{\pi\Phi}{2\Phi_0} = \pm 4\phi, \tag{7}$$

where the positive sign means the plaquette on the left of the directional hopping path has positive flux, and $\Phi_0 = h/e$.

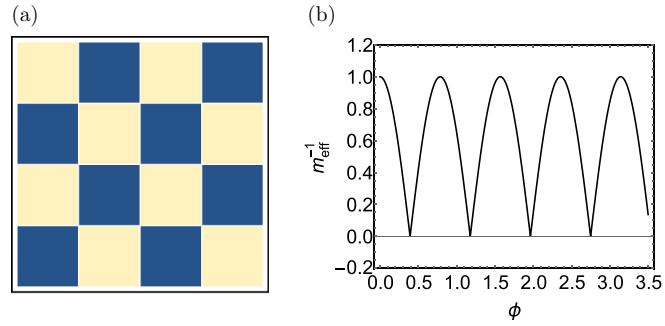

FIG. 4. (a) Tight-binding model on a square lattice with staggered magnetic fields for Schrödinger electrons. The xy axes are rotated by $\pi/4$ compared to that used for Eq. (2). (b) Inverse effective mass vs ϕ based on Eq. (8).

The momentum-space Hamiltonian can be easily diagonalized (see the Supplemental Material [74]). For any given ϕ, we can expand the two eigenenergies $\epsilon_\pm$ around small k, which gives

$$\epsilon_\pm(\mathbf{k}) \approx 4t \pm 2\sqrt{2 + 2\cos(8\phi)}t \mp \sqrt{\frac{1+\cos(8\phi)}{2}}\left(k_x^2 + k_y^2\right)a^2 t + O(k^3). \tag{8}$$

Thus, when $\phi \to \pi/8$, the quadratic term approaches zero, i.e., the low-energy band for long wavelengths becomes flat. The magic value is, therefore, $\frac{8\phi}{\pi} = \frac{\Phi}{\Phi_0} = 1$ or $\phi \approx 0.393$. At this value of ϕ, the eigenenergies are $\epsilon_\pm(\mathbf{k}) = 4t \pm 2t|\cos(k_x a) - \cos(k_y a)|$ where the second term vanishes along $k_x = \pm k_y$. The density of states (at $\epsilon = 4t$) does not diverge at this exact point because of the linear band touching along $k_x = \pm k_y$. It will, however, diverge when ϕ is infinitely close to $\pi/2$. The band structure and DOS can be found in the Supplemental Material [74].

Although the model gives a first magic value that is smaller than the first one shown in Fig. 2(b), it predicts a series of magic values,

$$\phi = \frac{(2n+1)\pi}{8}, \quad n \in \mathbb{Z}, \tag{9}$$

with the periodicity $\Delta\phi = \pi/4 \approx 0.785$, which is close to the period of the oscillation in Fig. 2(b). We, thus, believe that the recurring magic values in the original problem of the Schrödinger electrons should be due to the same reason as the magicness in the minimal model. Moreover, the latter can help us make connections with many early examples of flat-band lattice models [68–73] where the origin of the flat bands can be understood in terms of destructive interference. In the present case, the destructive interference comes from the values of ϕ in Eq. (9) at which $t_{ij} \equiv te^{i\varphi_{ij}} = -t_{ji}$ for nearest-neighbors i and j. Specifically, for some local wave function having equal weights on two diagonal sites of a plaquette, which belong to the same sublattice, hopping to their common nearest neighbors will cancel out. This is the reason for the complete flatness of the bands along $k_x = \pm k_y$. At distances much longer than the lattice period, such cancellation leads to strong suppression of hopping along almost all directions,

which is the reason for the vanishing inverse effective mass near $\mathbf{k} = 0$.

Plotting the inverse effective mass obtained from Eq. (9) vs ϕ gives Fig. 4(b), which is similar to Fig. 2(b) in terms of the oscillation. It fails, however, to capture some fine features in the latter, e.g., the negative values of m_{eff}^{-1} near the magic values, the decreasing amplitudes of the oscillation with increasing ϕ, etc., which is not surprising given the simplicity of the model. We do note that the decaying amplitude in Fig. 2(b) should be due to the general tendency of enhanced localization with increasing strength of the magnetic field. In the limit of the strong magnetic field, the eigenfunctions should be close to Landau orbits, and all bands are expected to be very flat.

We finally comment on the Dirac case. Because it is sufficient to use a single Gaussian-like Wannier function to describe the lowest band (for a given spin), the hopping parameters are real due to inversion symmetry. Thus, a minimal model for it [more exactly for $(H^D)^2$] should be a nearest-neighbor hopping model on a square lattice with one site per unit cell. Such a trivial model obviously cannot describe the band flattening as it stands, unless one allows the hopping amplitude to depend on ϕ which is *a posteriori*. Physically, the decreasing hopping with increasing ϕ should have two origins. The first is the Landau localization mentioned above. The second, which is unique to Dirac electrons, is the localization due to the Zeeman potential (last term in Eq. (21) of the Supplemental Material [74]), which has a Berry phase origin.

V. ZEEMAN COUPLING AND FLAT-BAND CHERN INSULATORS

We now consider the Zeeman coupling between the 2DEG and the periodic magnetic field, which always accompanies the orbital coupling. As mentioned in the Supplemental Material [74], Dirac electrons in the present problem can be viewed as a special case of 2DEG plus Zeeman coupling with $gm/m_e = 2$, where g is the g factor, m is the effective mass of the 2DEG, and m_e is the free-electron mass. In common 2DEGs, this ratio can vary significantly depending on materials realization [84,85] and may even be tunable in a given system [57,86,87]. We, thus, take the Zeeman coupling strength gm/m_e as a variable and study how the flat-band behaviors of Schrödinger and Dirac electrons can be smoothly bridged by changing it between 0 and 2.

Figure 5(a) shows the phase diagram of the inverse effective-mass m_{eff}^{-1} (in units of m^{-1}) at $\mathbf{k} = 0$ vs ϕ and gm/m_e. One can see that, along the horizontal line of $gm/m_e = 0$, i.e., pure Schrödinger without Zeeman coupling, m_{eff}^{-1} oscillates between positive (red color) and negative (blue color) values, and reaches 0 (white color) at magic values of ϕ. This is basically the same as Fig. 2(b). Similarly, when $gm/m_e = 2$, the figure reproduces the monotonic decay of m_{eff}^{-1} for the Dirac case shown in Fig. 1(b). In between these two limits, the regions with negative m_{eff}^{-1} form bands which start from being perpendicular to the ϕ axis when $gm/m_e = 0$ and gradually bend toward the horizontal $gm/m_e = 2$ line as gm/m_e increases. Accordingly, the lines of magic values of ϕ and gm/m_e, defined by $m_{\text{eff}}^{-1} = 0$, also bend to $gm/m_e = 2$ and disappear from the field of view.

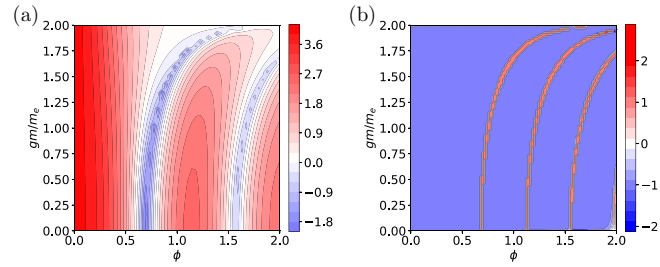

FIG. 5. (a) Inverse effective mass at $\mathbf{k} = 0$ and (b) Chern number of the up spin for the lowest band vs gm/m_e and ϕ. $K_c = 5\ K$. Brillouin-zone discretization of 11×11 and 10×10 were used for calculating m_{eff}^{-1} and the Chern number, respectively.

In the Supplemental Material [74], we have constructed a minimal three-band model, based on the Wannier functions, to qualitatively capture the band-flattening behavior for general values of gm/m_e. Interestingly, we find that the lowest band of the model quite generally has a nonzero Chern number, making it similar to the Haldane model of quantum anomalous Hall effect with a zero net magnetic field [88] but on the square lattice instead of the honeycomb lattice. Such an observation motivates us to calculate the Chern number of the lowest-band $\mathcal{C}_1$ (see the Supplemental Material [74]) in a 2D parameter space spanned by ϕ and gm/m_e and to see if, in the original problem, the flat bands can also be topologically nontrivial.

The phase diagram of the Chern number, shown in Fig. 5(b), is somewhat surprising since the Chern insulator phase is ubiquitous. Most regions have a $\mathcal{C}_1 = -1$ whereas on several narrow bands it is $+1$. These regions are separated by lines corresponding to band touching where the Chern number is ill defined. Comparing Figs. 5(a) and 5(b), one can see that the $\mathcal{C}_1 = 1$ regions coincide with places where m_{eff}^{-1} is extremal, indicating that there is band inversion near these values of m_{eff}^{-1}. Most importantly, the regions with zero or vanishingly small m_{eff}^{-1} almost all have nonzero $\mathcal{C}_1$. Thus, by tuning to the magic values of ϕ and gm/m_e, one could have flat bands and nontrivial topology simultaneously.

The above results have a caveat, however, due to spin degeneracy. The Schrödinger Hamiltonian with the Zeeman term included has an emergent symmetry $T_{(\pi,\pi)} \otimes \mathcal{K}$, where $\mathcal{K}$ is complex conjugation and $T_{(\pi,\pi)}$ is a real-space translation by $(\pi/K, \pi/K)$. Such a symmetry transforms the spin-up part of the Hamiltonian to the spin-down part and vice versa and is the reason for the double degeneracy of the spinful bands. Since the Chern number changes sign under complex conjugation, the two-spin species of a given band should always have opposite Chern numbers. This makes the net charge Chern number of a spinful band vanish but not the spin Chern number, which is the difference between the Chern numbers of opposite spins. We note that the vanishing of the net Chern number of a spinful band is a consequence of the high symmetry of the present model rather than a fundamental constraint. For example, adding a periodic scalar potential commensurate with the periodic magnetic field can have the same effect as the Zeeman potential for a single spin and can, thus, make the net Chern number of the lowest band nonzero.

VI. DISCUSSION AND CONCLUSION

The magnetic field used above has a very simple form [49–52]. In reality, magnetic fields created by periodic arrays of bar magnets or superconducting wires will have more Fourier components as well as finite in-plane magnetic fields. However, on one hand, the sinusoidal potential can be viewed as a legitimate first approximation if the spatial profile of the magnetic field is smooth [49–52]. On the other hand, we expect the general low-energy behavior of Dirac electrons or 2DEG revealed in this paper to qualitatively hold even with more realistic potential profiles, including that due to the pseudomagnetic fields created by strain in graphene [35,89–91]. For example, Schrödinger electrons will be likely to exhibit magicness since their low-energy Wannier orbitals should localize near zero-field lines, which will lead to complex hopping that periodically changes with field strength. To prove this, we have performed calculations for periodic Gaussian magnetic fields (for 2DEG) and periodic Gaussian strain fields (for Dirac electrons) [89–91] (Fig. 3 in the Supplemental Material [74]). The calculations could only be performed using the real-space method explained in the Supplemental Material [74] since there are infinitely many Fourier components. The results strongly resemble those for the simple cosinusoidal fields. Namely, in the Dirac case, the velocity monotonically decreases, whereas, in the Schrödinger case, the inverse effective mass repeatedly crosses zero.

The typical strength of fields needed to get flat bands should be such that the magnetic flux through each plaquette is on the order of Φ_0. We emphasize that this is a rather modest requirement (with additional constraint from the disorder potential explained below) especially for large periods or small K. Since $\Phi_0 \approx 4.136 \times 10^{-3}\ \mathrm{T}\,\mu\mathrm{m}^2$, a micrometer period field only needs to have an amplitude $\sim 10^2$ G. In the case of graphene, such long wavelengths also mean the two valleys of graphene can be viewed as independent [92,93]. Based on the lessons learned from the twisted multilayer graphene systems, for interaction-driven phases to appear, the number of moiré unit cells in a given sample does not have to be macroscopically large—$10^2 \times 10^2$ is sufficient. Artificial superlattices with such numbers of periods are not out of reach [49,50,54–57]. Experimentally, one can use either transport [54–56,59–61] or spectroscopic [92] methods to reveal the existence of the flat bands [9,10,12,13] and to look for exotic phases at very low temperatures. The complex hopping in the tight-binding models is reminiscent of the loop-current model for cuprates [94,95], thus, suggesting potential new phases more proximate to high-temperature superconductors on a square lattice.

Disorder places another constraint on the lower bound of the magnetic field or the upper bound of the spatial period. For the Bloch wave picture to be valid, the kinetic energy of the electron must be larger than the disorder potential denoted by Γ. For a given spatial period $2\pi/K$, the consideration above suggests the width of the lowest-energy band (or lowest positive energy band for the Dirac case) must be, at least, larger than the disorder potential when the magnetic field is weak. This requires $\hbar^2K^2/2m > \Gamma$ for 2DEG and $\hbar v_F K > \Gamma$ for Dirac electrons and, consequently, gives a lower bound of the magnetic field if $\phi \sim 1$. For Dirac electrons, in the case of graphene, $\Gamma \sim 1$ meV if we adopt the experimental relaxation time of 3.0×10^{-13} s [96]. Thus, $K \geqslant 1.67 \times 10^{-3}\ \mathrm{nm}^{-1}$, or the period must be smaller than 3.8 μm and $B \geqslant 3.7$ mT for achieving nearly flat bands ($\phi \sim 2$). For high mobility 2DEG, such as GaAs/AlGaAs, $\Gamma \sim 0.01$ meV if using the mobility $\mu = 70\ \mathrm{m}^2\,\mathrm{V}^{-1}\,\mathrm{s}^{-1}$ [97] and the effective-mass $0.067m_e$. This corresponds to a lower bound $K \geqslant 4.6 \times 10^{-3}\ \mathrm{nm}^{-1}$ (or a period of 1.4 μm) and $B \geqslant 8.6$ mT for achieving nearly flat bands ($\phi \sim 0.6$). These values of B are, at least, one order of magnitude smaller than that achieved experimentally for smooth spatial modulations of the real magnetic field [49,50,98–102] or strain [35,89–91], and the micrometer period is experimentally realizable [49,50,98–102].

Although our prescription works for the whole spectrum bridging Dirac materials and 2DEG, the former can take advantage of the various pseudomagnetic fields through, e.g., periodic strain or Zeeman field that may be easier to implement experimentally. Moreover, practically the absence of magicness in the Dirac case makes it much easier to realize flat bands without the need of fine-tuning. In contrast, in the twisted multilayer graphene systems, the magicness requires not only precise control of the twisting angle, but also that of its spatially uniformity. On a side note since the continuum description of graphene moiré also has the form of Dirac electrons subject to non-Abelian gauge potentials [29–31], it is possible to use similar arguments to understand the origin of the moiré flat bands as well.

Although we have been focusing on periodic magnetic fields, band flattening as a general trend should be common for periodic potentials getting stronger and stronger. Even for Dirac electrons which are known to be difficult to confine with scalar potential wells, periodic scalar potentials can still lead to 1D flat bands [92,93]. Finally, weak periodic electric potentials can be used together with a periodic magnetic field on 2DEG to get the ubiquitous Chern insulator phase.

In conclusion, we find that spatially periodic magnetic fields can be a practical and versatile approach to realizing emergent flat-band lattices with different superlattice symmetries. The contrasting band-flattening behaviors of Dirac (no magicness) and Schrödinger (with magicness) electrons can be understood through different minimal tight-binding models based on their respective Wannier functions localized by the periodic magnetic fields. In particular, the magicness in the Schrödinger case is due to a complex hopping amplitude along zero-field lines whose phase changes periodically with increasing field. The two limiting cases can be interpolated by considering the Zeeman coupling between the spin degrees of freedom of a 2DEG and the magnetic field and by varying the g factor or the effective mass. The Zeeman coupling also quite generally leads to topologically nontrivial flat bands with nonzero Chern numbers for each spin. Future experimental and theoretical studies on this platform, which is a powerful alternative to the moiré system, may reveal more exotic phases when interaction is taken into account.

ACKNOWLEDGMENTS

M.T. and H.C. were supported by the start-up funding of CSU. O.P. is supported by NSF CAREER Grant No. DMS-1452349. The authors are grateful to A. MacDonald, Q. Niu, D. Xiao, F. Peeters, and P. Jarillo-Herrero for helpful discussions.

[1] J. Hass, F. Varchon, J. E. Millán-Otoya, M. Sprinkle, N. Sharma, W. A. de Heer, C. Berger, P. N. First, L. Magaud, and E. H. Conrad, Phys. Rev. Lett. **100**, 125504 (2008).

[2] C. R. Dean, A. F. Young, I. Meric, C. Lee, L. Wang, S. Sorgenfrei, K. Watanabe, T. Taniguchi, P. Kim, K. L. J. Shepard, and J. Hone, Nat. Nanotechnol. **5**, 722 (2010).

[3] J. Xue, J. Sanchez-Yamagishi, D. Bulmash, P. Jacquod, A. Deshpande, K. Watanabe, T. Taniguchi, P. Jarillo-Herrero, and B. J. LeRoy, Nature Mater. **10**, 282 (2011).

[4] E. Wang, X. Lu, S. Ding, W. Yao, M. Yan, G. Wan, K. Deng, S. Wang, G. Chen, L. Ma, J. Jung, A. V. Fedorov, Y. Zhang, G. Zhang, and S. Zhou, Nat. Phys. **12**, 1111 (2016).

[5] C. Zhang, C.-P. Chuu, X. Ren, M.-Y. Li, L.-J. Li, C. Jin, M.-Y. Chou, and C.-K. Shih, Sci. Adv. **3**, e1601459 (2017).

[6] J. M. B. Lopes dos Santos, N. M. R. Peres, and A. H. Castro Neto, Phys. Rev. Lett. **99**, 256802 (2007).

[7] E. J. Mele, Phys. Rev. B **81**, 161405(R) (2010).

[8] R. Bistritzer and A. H. MacDonald, Proc. Natl. Acad. Sci. USA **108**, 12233 (2011).

[9] Y. Cao, V. Fatemi, A. Demir, S. Fang, S. L. Tomarken, J. Y. Luo, J. D. Sanchez-Yamagishi, K. Watanabe, T. Taniguchi, E. Kaxiras, R. C. Ashoori, and P. Jarillo-Herrero, Nature (London) **556**, 80 (2018).

[10] Y. Cao, V. Fatemi, S. Fang, K. Watanabe, T. Taniguchi, E. Kaxiras, and P. Jarillo-Herrero, Nature (London) **556**, 43 (2018).

[11] M. Yankowitz, S. Chen, H. Polshyn, Y. Zhang, K. Watanabe, T. Taniguchi, D. Graf, A. F. Young, and C. R. Dean, Science **363**, 1059 (2019).

[12] D. Pierucci, H. Sediri, M. Hajlaoui, J.-C. Girard, T. Brumme, M. Calandra, E. Velez-Fort, G. Patriarche, M. G. Silly, G. Ferro, V. Souliére, M. Marangolo, F. Sirotti, F. Mauri, and A. Ouerghi, ACS Nano **9**, 5432 (2015).

[13] B. L. Chittari, G. Chen, Y. Zhang, F. Wang, and J. Jung, Phys. Rev. Lett. **122**, 016401 (2019).

[14] G. E. Volovik, JETP Lett. **107**, 516 (2018).

[15] C. Xu and L. Balents, Phys. Rev. Lett. **121**, 087001 (2018).

[16] A. M. DaSilva, J. Jung, and A. H. MacDonald, Phys. Rev. Lett. **117**, 036802 (2016).

[17] G. Baskaran, arXiv:1804.00627.

[18] J. F. Dodaro, S. A. Kivelson, Y. Schattner, X. Q. Sun, and C. Wang, Phys. Rev. B **98**, 075154 (2018).

[19] J. González and T. Stauber, Phys. Rev. Lett. **122**, 026801 (2019).

[20] H. Guo, X. Zhu, S. Feng, and R. T. Scalettar, Phys. Rev. B **97**, 235453 (2018).

[21] E. Laksonoa, J. N. Leawa, A. Reavesc, M. Singhc, X. Wanga, S. Adama, and X. Gu, Solid State Commun. **282**, 38 (2018).

[22] C.-C. Liu, L.-D. Zhang, W.-Q. Chen, and F. Yang, Phys. Rev. Lett. **121**, 217001 (2018).

[23] H. C. Po, L. Zou, A. Vishwanath, and T. Senthil, Phys. Rev. X **8**, 031089 (2018).

[24] S. Ray, J. Jung, and T. Das, Phys. Rev. B **99**, 134515 (2019).

[25] A. Thomson, S. Chatterjee, S. Sachdev, and M. S. Scheurer, Phys. Rev. B **98**, 075109 (2018).

[26] F. Wu, A. H. MacDonald, and I. Martin, Phys. Rev. Lett. **121**, 257001 (2018).

[27] X. Y. Xu, K. T. Law, and P. A. Lee, Phys. Rev. B **98**, 121406(R) (2018).

[28] N. F. Q. Yuan and L. Fu, Phys. Rev. B **98**, 045103 (2018).

[29] P. San-Jose, J. González, and F. Guinea, Phys. Rev. Lett. **108**, 216802 (2012).

[30] L.-J. Yin, J.-B. Qiao, W.-J. Zuo, W.-T. Li, and L. He, Phys. Rev. B **92**, 081406(R) (2015).

[31] J. González, Phys. Rev. B **94**, 165401 (2016).

[32] N. Levy, S. A. Burke, K. L. Meaker, M. Panlasigui, A. Zettl, F. Guinea, A. H. C. Neto, and M. F. Crommie, Science **329**, 544 (2010).

[33] E. Tang and L. Fu, Nat. Phys. **10**, 964 (2014).

[34] M. A. Mueed, Md. S. Hossain, I. Jo, L. N. Pfeiffer, K. W. West, K. W. Baldwin, and M. Shayegan, Phys. Rev. Lett. **121**, 036802 (2018).

[35] J. Mao, S. P. Milovanović, M. Anđelković, X. Lai, Y. Cao, K. Watanabe, T. Taniguchi, L. Covaci, F. M. Peeters, A. K. Geim, Y. Jiang, and E. Y. Andrei, arXiv:2006.01660v1.

[36] D. Weiss, K. V. Klitzing, K. Ploog, and G. Weimann, Europhys. Lett. **8**, 179 (1989).

[37] R. R. Gerhardts, D. Weiss, and K. v. Klitzing, Phys. Rev. Lett. **62**, 1173 (1989).

[38] R. W. Winkler, J. P. Kotthaus, and K. Ploog, Phys. Rev. Lett. **62**, 1177 (1989).

[39] C. W. J. Beenakker, Phys. Rev. Lett. **62**, 2020 (1989).

[40] P. Vasilopoulos and F. M. Peeters, Phys. Rev. Lett. **63**, 2120 (1989).

[41] R. R. Gerhardts, D. Weiss, and U. Wulf, Phys. Rev. B **43**, 5192 (1991).

[42] C. Albrecht, J. H. Smet, K. von Klitzing, D. Weiss, V. Umansky, and H. Schweizer, Phys. Rev. Lett. **86**, 147 (2001).

[43] M. C. Geisler, J. H. Smet, V. Umansky, K. von Klitzing, B. Naundorf, R. Ketzmerick, and H. Schweizer, Phys. Rev. Lett. **92**, 256801 (2004).

[44] X. F. Wang, P. Vasilopoulos, and F. M. Peeters, Phys. Rev. B **69**, 035331 (2004).

[45] C. Albrecht, J. H. Smet, D. Weiss, K. von Klitzing, R. Hennig, M. Langenbuch, M. Suhrke, U. Rössler, V. Umansky, and H. Schweizer, Phys. Rev. Lett. **83**, 2234 (1999).

[46] S. Chowdhury, C. J. Emeleus, B. Milton, E. Skuras, A. R. Long, J. H. Davies, G. Pennelli, and C. R. Stanley, Phys. Rev. B **62**, 4821(R) (2000).

[47] S. Chowdhury, A. R. Long, E. Skuras, J. H. Davies, K. Lister, G. Pennelli, and C. R. Stanley, Phys. Rev. B **69**, 035330 (2004).

[48] Y. Kato, A. Endo, S. Katsumoto, and Y. Iye, Phys. Rev. B **86**, 235315 (2012).

[49] H. A. Carmona, A. K. Geim, A. Nogaret, P. C. Main, T. J. Foster, M. Henini, S. P. Beaumont, and M. G. Blamire, Phys. Rev. Lett. **74**, 3009 (1995).

[50] P. D. Ye, D. Weiss, R. R. Gerhardts, M. Seeger, K. von Klitzing, K. Eberl, and H. Nickel, Phys. Rev. Lett. **74**, 3013 (1995).

[51] D. P. Xue and G. Xiao, Phys. Rev. B **45**, 5986 (1992).

[52] F. M. Peeters and P. Vasilopoulos, Phys. Rev. B **47**, 1466 (1993).

[53] M. C. Chang and Q. Niu, Phys. Rev. B **50**, 10843 (1994).

[54] P. D. Ye, D. Weiss, K. v. Klitzing, and K. Eberl, Appl. Phys. Lett. **67**, 1441 (1995).

[55] P. D. Ye, D. Weiss, and R. R. Gerhardts, J. Appl. Phys. **81**, 5444 (1997).

[56] E. Skuras, A. R. Long, S. Chowdhury, and M. Rahman, J. Appl. Phys. **90**, 2623 (2001).

[57] C. Betthausen, T. Dollinger, H. Saarikoski, V. Kolkovsky, G. Karczewski, T. Wojtowicz, K. Richter, and D. Weiss, Science **337**, 324 (2012).

[58] M. Drienovsky, J. Joachimsmeyer, A. Sandner, M.-H. Liu, T. Taniguchi, K. Watanabe, K. Richter, D. Weiss, and J. Eroms, Phys. Rev. Lett. **121**, 026806 (2018).

[59] L. A. Ponomarenko, R. V. Gorbachev, G. L. Yu, D. C. Elias, R. Jalil, A. A. Patel, A. Mishchenko, A. S. Mayorov, C. R. Woods, J. R. Wallbank, M. Mucha-Kruczynski, B. A. Piot, M. Potemski, I. V. Grigorieva, K. S. Novoselov, F. Guinea, V. I. Falko, and A. K. Geim, Nature (London) **497**, 594 (2013).

[60] C. R. Dean, L. Wang, P. Maher, C. Forsythe, F. Ghahari, Y. Gao, J. Katoch, M. Ishigami, P. Moon, M. Koshino, T. Taniguchi, K. Watanabe, K. L. Shepard, J. Hone, and P. Kim, Nature (London) **497**, 598 (2013).

[61] R. K. Kumar, A. Mishchenko, X. Chen, S. Pezzini, G. H. Auton, L. A. Ponomarenko, U. Zeitler, L. Eaves, V. I. Falko, and A. K. Geim, Proc. Natl. Acad. Sci. USA **115**, 5135 (2018).

[62] I. S. Ibrahim and F. M. Peeters, Phys. Rev. B **52**, 17321 (1995).

[63] Y. H. Chiu, Y. H. Lai, J. H. Ho, D. S. Chuu, and M. F. Lin, Phys. Rev. B **77**, 045407 (2008).

[64] L. Dell'Anna and A. De Martino, Phys. Rev. B **79**, 045420 (2009).

[65] M. R. Masir, P. Vasilopoulos, and F. M. Peeters, New J. Phys. **11**, 095009 (2009).

[66] L. Z. Tan, C.-H. Park, and S. G. Louie, Phys. Rev. B **81**, 195426 (2010).

[67] M. Taillefumier, V. K. Dugaev, B. Canals, C. Lacroix, and P. Bruno, Phys. Rev. B **84**, 085427 (2011).

[68] B. Sutherland, Phys. Rev. B **34**, 5208 (1986).

[69] E. H. Lieb, Phys. Rev. Lett. **62**, 1201 (1989).

[70] A. Mielke, J. Phys. A **24**, L73 (1991).

[71] A. Mielke, J. Phys. A **24**, 3311 (1991).

[72] H. Tasaki, Phys. Rev. Lett. **69**, 1608 (1992).

[73] H. Tasaki, Eur. Phys. J. B **64**, 365 (2008).

[74] See Supplemental Material at http://link.aps.org/supplemental/10.1103/PhysRevB.102.035425 for additional details, which includes Refs. [103–111].

[75] J. M. B. Lopes dos Santos, N. M. R. Peres, and A. H. Castro Neto, Phys. Rev. B **86**, 155449 (2012).

[76] R. Jackiw, Phys. Rev. D **29**, 2375 (1984).

[77] I. Snyman, Phys. Rev. B **80**, 054303 (2009).

[78] G. Allaire and A. Piatnitski, Commun. Math. Phys. **258**, 1 (2005).

[79] L. Barletti and N. Ben Abdallah, Commun. Math. Phys. **307**, 567 (2011).

[80] H. Chen, O. Pinaud, and M. Tahir, arXiv:2005.14340.

[81] J. M. Luttinger, Phys. Rev. **84**, 814 (1951).

[82] G. H. Wannier, Rev. Mod. Phys. **34**, 645 (1962).

[83] E. I. Blount, Phys. Rev. **126**, 1636 (1962).

[84] S. Adachi, J. Appl. Phys. **53**, 8775 (1982).

[85] A. A. Taskin and Y. Ando, Phys. Rev. B **84**, 035301 (2011).

[86] A. Giorgioni, S. Paleari, S. Cecchi, E. Vitiello, E. Grilli, G. Isella, W. Jantsch, M. Fanciulli, and F. Pezzoli, Nat. Commun. **7**, 13886 (2016).

[87] Z. Wang, Z. Zhong, X. Hao, S. Gerhold, B. Stöger, M. Schmid, J. Sánchez-Barriga, A. Varykhalov, C. Franchini, K. Held, and U. Diebold, Proc. Natl. Acad. Sci. USA **111**, 3933 (2014).

[88] F. D. M. Haldane, Phys. Rev. Lett. **61**, 2015 (1988).

[89] A. H. Castro Neto, F. Guinea, N. M. R. Peres, K. S. Novoselov, and A. K. Geim, Rev. Mod. Phys. **81**, 109 (2009).

[90] F. Guinea, M. I. Katsnelson, and A. K. Geim, Nat. Phys. **6**, 30 (2010).

[91] D. Zhai and N. Sandler, Mod. Phys. Lett. B **33**, 1930001 (2019).

[92] M. Yankowitz, J. Xue, D. Cormode, J. D. Sanchez-Yamagishi, K. Watanabe, T. Taniguchi, P. Jarillo-Herrero, P. Jacquod, and B. J. LeRoy, Nat. Phys. **8**, 382 (2012).

[93] C.-H. Park, L. Yang, Y.-W. Son, M. L. Cohen, and S. G. Louie, Nat. Phys. **4**, 213 (2008).

[94] C. M. Varma, Phys. Rev. B **55**, 14554 (1997).

[95] C. M. Varma, Phys. Rev. B **73**, 155113 (2006).

[96] T. Stauber, N. M. R. Peres, and F. Guinea, Phys. Rev. B **76**, 205423 (2007).

[97] A. Endo and Y. Iye, J. Phys. Soc. Jpn. **77**, 064713 (2008).

[98] K. S. Novoselov, A. K. Geim, S. V. Dubonos, Y. G. Cornelissens, F. M. Peeters, and J. C. Maan, Phys. Rev. B **65**, 233312 (2002).

[99] A. Nogaret, D. N. Lawton, D. K. Maude, J. C. Portal, and M. Henini, Phys. Rev. B **67**, 165317 (2003).

[100] A. Tarasov, S. Hugger, H. Xu, M. Cerchez, T. Heinzel, I. V. Zozoulenko, U. Gasser-Szerer, D. Reuter, and A. D. Wieck, Phys. Rev. Lett. **104**, 186801 (2010).

[101] A. Nogaret, J. Phys.: Condens. Matter **22**, 253201 (2010).

[102] A. Leuschner, J. Schluck, M. Cerchez, T. Heinzel, K. Pierz, and H. W. Schumacher, Phys. Rev. B **95**, 155440 (2017).

[103] R. Hammer, W. Potz, and A. Arnold, J. Comput. Phys. **256**, 728 (2014).

[104] R. Hammer, W. Potz, and A. Arnold, J. Comput. Phys. **265**, 50 (2014).

[105] C.-H. Park, N. Bonini, T. Sohier, G. Samsonidze, B. Kozinsky, M. Calandra, F. Mauri, and N. Marzari, Nano Lett. **14**, 1113 (2014).

[106] T. Sohier, M. Calandra, C.-H. Park, N. Bonini, N. Marzari, and F. Mauri, Phys. Rev. B **90**, 125414 (2014).

[107] W. Kohn, Phys. Rev. **115**, 809 (1959).

[108] G. Nenciu, Commun. Math. Phys. **91**, 81 (1983).

[109] C. Brouder, G. Panati, M. Calandra, C. Mourougane, and N. Marzari, Phys. Rev. Lett. **98**, 046402 (2007).

[110] N. Marzari and D. Vanderbilt, Phys. Rev. B **56**, 12847 (1997).

[111] T. Fukui, Y. Hatsugai, and H. Suzuki, J. Phys. Soc. Jpn. **74**, 1674 (2005).